Ab initio study of CsI and its surface

R. M. Ribeiro*
Centro de Física, Universidade do Minho, Campus de Gualtar, 4710-057 Braga, Portugal

J. Coutinho and V. J. B. Torres
Departamento de Física, Universidade de Aveiro, Campus Santiago, 3810-193 Aveiro, Portugal

R. Jones and S. J. Sque
School of Physics, University of Exeter, Stocker Road, EX4 4QL, United Kingdom

S. Öberg
Department of Mathematics, Luleå University of Technology, Luleå S-97187, Sweden

M. J. Shaw and P. R. Briddon
School of Natural Sciences, University of Newcastle upon Tyne, Newcastle upon Tyne, NE1 7RU, United Kingdom
(Received 16 April 2006; revised manuscript received 21 June 2006; published 27 July 2006)

Cesium iodide properties, both in the bulk and on (110) and (100) surfaces, are studied using density functional theory. The bulk lattice constant, bulk modulus, and elastic constants are in good agreement with the experimental values. The electronic band structure is also calculated, as well as the density of states. On the surfaces, relaxation of the atoms was performed, and the atomic geometry and electronic structure have been studied.

DOI: 10.1103/PhysRevB.74.035430 PACS number(s): 68.35.Bs, 71.15.Mb, 73.20.At

I. INTRODUCTION

Cesium iodide is being extensively used for its properties as a scintillator, especially when doped with thallium. In recent years it has also been used in RICH detectors, and the High Momentum Particle IDentification (HMPID) system of ALICE at LHC (CERN) is based on a CsI-RICH detector, aiming at charged π/K/p identification.[1] The increasing interest in CsI stems from a number of favorable properties for photoconverters: i.e., (i) the high quantum efficiency that can be achieved in CsI photocathodes [as high as 35%–40% (Ref. 2)], making CsI the alkali halide with the highest quantum efficiency, (ii) the lowest electron affinity (of the order of 0.1–0.2 eV), and (iii) an electron escape length as large as ~16 nm for 1-eV electrons (see Ref. 3 and references therein).

Major problems in CsI RICH detectors arise from its degradation on exposure to air due to the strong affinity of CsI to water, the illumination by an intense photon flux, and its ageeing during operation due to exposure to ionizing radiation.[4] In the first case, a short exposure to air of a few hours can be recovered by a subsequent annealing in vacuum.[5] Photon flux need to be very intense ($\geqslant 10^{12}$ cm^{-2} s^{-1}) in order to damage the detector.[6] The ionizing radiation is caused by the ions produced in the gaseous avalanches, which bombard the CsI layer of the detector.[6] These mechanisms are not yet very well understood, and atomistic calculations are needed to better understand them.[6]

In this context, understanding the properties of CsI surfaces is very important to grasp the degradation processes. Yet not many atomistic studies of the CsI surface are available in the literature. Jockisch *et al.*[7] studied the properties of the {110} surfaces of cesium halides, including CsI, at the atomic level, using a shell model. They obtained relaxation of the (110) CsI surface and its dynamics, but they calculated no electronic surface states or considered other surfaces. On the other hand, several studies were performed on bulk CsI, both theoretical[8–16] and experimental.[11,17–22] Their results will be discussed in the following text, along with our results.

Also missing is a study of adsorbates (especially water), how they interact with the surface, and the process of CsI dissolution and surface modification due to adsorbates. In this work we report on total-energy density-functional-theory (DFT) calculations of bulk CsI and its surfaces, paying particular attention to their fully relaxed electronic and atomic structure. The paper is organized as follows: in Sec. II we introduce the calculational details. The main results are reported in Sec. III, where we discuss the calculations in the bulk CsI, (110) surface, and (100) surface (Secs. III A, III B 1, and III B 2, respectively). Finally, in Sec. IV we present the conclusions.

II. THEORETICAL METHOD

All calculations are performed with an *ab initio* spin-density-functional code (AIMPRO),[23,24] along with the generalized gradient approximation (GGA) according to Perdew, Burke, and Ernzerhof.[25] For the Cs atom, the 5*s*, 5*p*, and 6*s* levels are treated explicitly as valence states, whereas for iodine we consider the 5*s* and 5*p* states. Lower states (core states) are accounted for by using the dual-space separable pseudopotentials by Hartwigsen, Goedecker, and Hutter.[26] The valence states are expanded over a set of *s*-, *p*-, and *d*-like Cartesian-Gaussian Bloch functions,

TABLE I. Lattice constant (Å), bulk modulus (GPa) and its pressure derivative for CsI calculated by several authors. Experimental values of a_0, B, and B' are 4.567 Å, 11.9 GPa, and 5.93, respectively (see Ref. 11). Values in parentheses are percentages of the experimental values.

Work	Method	a_0	B	B'
This work	DFT, GGA	4.635 (+1.49)	12.21 (+2.14)	4.39 (-26)
Winkler and Milman[a]	DFT, GGA	4.636 (+1.50)	13.5 (+13.4)	3.6 (−39)
Cortona[b]	DFT, LDA	4.52 (−1.00)	13.6 (+14.3)	
Winkler[a]	DFT, LDA	4.411 (−3.50)		
Baroni and Giannezzi[c]	DFT, LDA	4.45 (−2.56)	11.0 (−7.56)	5.8 (−2.2)
Mei*et al.*	DFT, LDA	4.33 (−5.19)	17.1 (+43)	
Satpathy[d]	Rel., LDA	4.475 (−2.00)	11.1 (−6.72)	6.4 (+7.9)
Cortona[b]	Rel., LDA	4.50 (−1.46)	14.4 (+21.0)	
Aidun *et al.*[e]	APW, LDA	4.529 (−0.83)	11.95 (+0.40)	6.14 (+3.5)

[a]Reference 8.
[b]Reference 9.
[c]Reference 10.
[d]Reference 11.
[e]Reference 12.
[f]Reference 29.

$$B_{\mathbf{k}i}(\mathbf{r}) = \frac{1}{\sqrt{N_{\mathbf{L}}}} \sum_{\mathbf{n}}^{N_{\mathbf{L}}} \phi_i(\mathbf{r} - \mathbf{R}_i - \mathbf{L}_{\mathbf{n}}) \exp(i\mathbf{k} \cdot \mathbf{L}_{\mathbf{n}}), \tag{1}$$

over N_L supercell lattice sites. The localized orbitals for the atom located at $\mathbf{R}_i$ are given by

$$\phi_i(\mathbf{r}) = (x - R_{ix})^{l_1}(y - R_{iy})^{l_2}(z - R_{iz})^{l_3} \exp[-a_i|\mathbf{r} - \mathbf{R}_i|^2], \tag{2}$$

where $l_i \geqslant 0$, and s, p, and d orbitals correspond to $\Sigma_i\, l_i = 0$, 1, or 2, respectively. Exponent values (a_i) were optimized in order to give the lowest energy for bulk CsI. A total of 30 and 24 ϕ_i functions are placed on every cesium and iodine atoms, respectively. Kohn-Sham states are then expressed as linear combinations of basis functions,

$$\psi_{\mathbf{k}\lambda}(\mathbf{r}) = \sum_i c_{\lambda \mathbf{k}i} B_{\mathbf{k}i}(\mathbf{r}), \tag{3}$$

and the electron density is readily obtained as

TABLE II. Elastic constants both calculated and experimental. The experimental values show the interval of values measured by different authors (see Refs. 17–21).

Elastic constant	This work (GPa)	Ghosh and Basn[a] (GPa)	Mei *et al.*[b] (GPa)	Experimental (GPa)
c_{11}	25.708	26.94	32.6	24.34–27.46
c_{12}	5.360	8.37	9.4	6.36–7.9
c_{44}	5.523	10.92	5.0	6.24–8.7

[a]Reference 13.
[b]Reference 29.

$$n(\mathbf{r}) = \sum_{i,j,\mathbf{k}} b_{ij}(\mathbf{k}) B^*_{\mathbf{k}i}(\mathbf{r}) B_{\mathbf{k}j}(\mathbf{r}), \tag{4}$$

with

$$b_{ij}(\mathbf{k}) = \sum_{\lambda} f_{\mathbf{k}\lambda} c^*_{\mathbf{k}\lambda i} c_{\mathbf{k}\lambda j}, \tag{5}$$

where $f_{\mathbf{k}\lambda}$ is the occupancy of the $\mathbf{k}\lambda$ state. The calculation of potential terms is more efficient in reciprocal space, and therefore the electron density is Fourier transformed by using plane waves with kinetic energy of up to 300 Ry. Each sur-

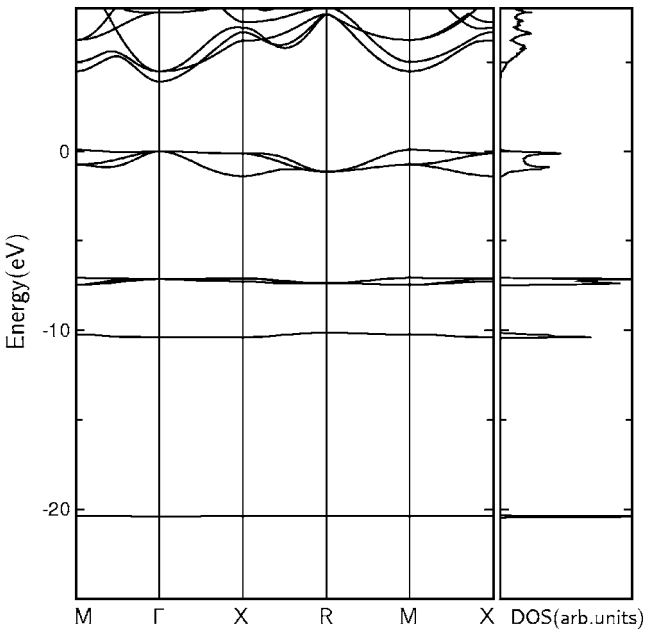

FIG. 1. Electronic band structure and density of states (DOS) of bulk CsI. The zero value for energy was aligned with the valence band at the Γ point.

face was modeled in a slab geometry by including a vacuum region in a supercell, with the long edge of the cell aligned along [001]. Further details about the shape and number of atoms in the supercells are given in Sec. III B.

The Brillouin zone (BZ) was sampled according to the scheme proposed by Monkhorst and Pack.[27] Here a grid of equally distant **k** points is generated and folded according to the symmetry of the BZ. The sparcity of the grid depends on the shape and volume of the BZ. For the unit cell (two atoms), we used grids of up to $12\times12\times12$ points, whereas for the slab runs a $8\times8\times1$ grid. An increase in the number of points did not result in a significant total energy change.

III. RESULTS

A. Bulk CsI

The calculation of the total energy as a function of the cell volume, $E(V)$, was combined with the Murnaghan equation of state,[28]

$$E(V) = E_0 + \frac{BV}{B'}\left(\frac{(V_0/V)^{B'}}{B'-1}+1\right) - \frac{BV_0}{B'-1}, \tag{6}$$

to obtain the equilibrium cell volume (V_0), lattice constant (a_0), bulk modulus (B), and its pressure derivative (B').

The relaxed lattice parameter obtained for bulk CsI (CsCl structure) using the above parameters was $a_0=4.635$ Å, which is 1.49% off the experimental value of 4.567 Å.[11] This figure is comparable to that obtained by other authors (see Table I). It is well known that whereas the GGA to the exchange-correlation energy overestimates the experimental lattice parameter, the local density approximation (LDA) favors smaller bond lengths. The error of the calculations is typically 1%–2%.

The calculated bulk modulus $B=12.21$ GPa is only 2.14% off the experimental value of $B=11.9$ GPa. In fact, as Winkler and Milman[8] remark, the values given in the literature for the bulk modulus vary a lot, between 9.2 and 13.5 GPa. But the most measured value is 11.9 GPa or consistent with it.[11,30–33] Table I shows the result of this work compared with other calculations. It can be seen that the bulk modulus is in very good agreement with experiment, but its first derivative is not so good. The results from other authors are in general worse than this work, with large variations from author to author.

Elastic constants were also obtained (Table II) by applying several small strains to the lattice, determining the corresponding energies, and adjusting them to a parabola. Again, the experimental results show a significative variation,[17–21] and so we show in Table II the interval of values they obtained. Also shown are the calculated values obtained by Ghosh and Basu[13] using a deformable shell model, which are the only calculated values we could find in the literature. It can be seen that the value for the c_{11} fits very well in the interval of experimental values but the values of c_{12} and c_{44} fall short of the experimental values.

We calculated the bulk modulus using the elastic constants by the equation

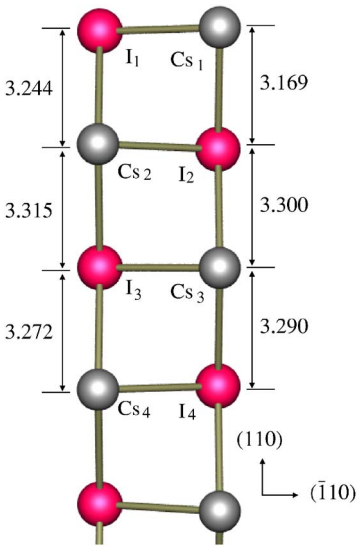

FIG. 2. (Color online) Diagram of the atoms near the (110) surface. The relevant atoms are labelled, and the numbers represent distances in Å.

$$B = \frac{c_{11}+2c_{12}}{3}, \tag{7}$$

and we obtained a value of 12.14 GPa, which is very close to the one obtained using Eq. (6).

The electronic band structure was calculated using a 2250-**k**-point sampling of the BZ, and the result is shown in Fig. 1. The band gap achieved was 3.91 eV, underestimated as is usual in DFT. The experimental value is 6.2 eV,[22] so we got 63% of the experimental value. Several early calculations of the band structure were previously reported: Onodera[14] and Rössler[34] used the non-self-consistent Korringa-Kohn-Rostoker Green's function method, while Aidun *et al.*[12] used a self-consistent nonrelativistic symmetrized-augmented-plane-wave calculation. Satpathy *et al.*[16] made an interesting comparison between relativistic and nonrelativistic calculations, using a linear-muffin-tin-orbital method in the atomic

TABLE III. Distances from the bulk equilibrium positions; a positive direction means moving away from the surface towards the vacuum. The atom labels refer to the ones shown in Fig. 2. Also shown are the values obtained by Jockisch *et al.*(see Ref. 7).

Atom	This work (Å)	Jockisch *et al.*[a] (Å)
Cs1	−0.089	−0.069
I1	0.017	0.016
Cs2	0.051	0.024
I2	0.020	−0.013
Cs3	−0.003	−0.008
I3	0.013	0.006
Cs4	0.001	0.003
I4	0.002	−0.002

[a]Reference 7.

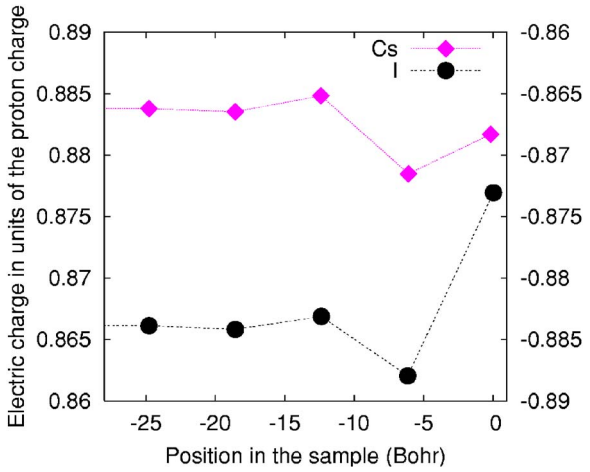

FIG. 3. (Color online) Charge state of Cs and I atoms, as a function of position in the material, as obtained from the Mulliken charge, for the (110) surface sample. The surface is at 0. The scale for iodine atoms is on the right and that for cesium atoms is on the left.

sphere approximation (LTMO-ASA). They found differences in the band structure—namely, a splitting of the set of highest occupied bands in two. Our results are in agreement with the nonrelativistic results, as it should be, and we get better results in the lattice constant and bulk modulus than Satpathy *et al.*[16] using relativistic approximations. Yet one has to remember that the inclusion of relativistic effects may affect the position of the surface states in the surface band calculations of Secs. III B 1 and III B 2.

We identified the three highest occupied wave functions at the Γ point as *p* type, localized near the iodine atoms. The next three occupied wave functions were also *p* type but localized near the cesium atoms. The lowest unoccupied level at the Γ point is *s* type and centered on both Cs and I atoms. The next unoccupied level is localized in between the atoms and fills most of the bulk space. The next levels are *d* type, centered on the cesium atoms.

The density of states (DOS) was calculated by sampling 125 000 points throughout the BZ. The result is shown in

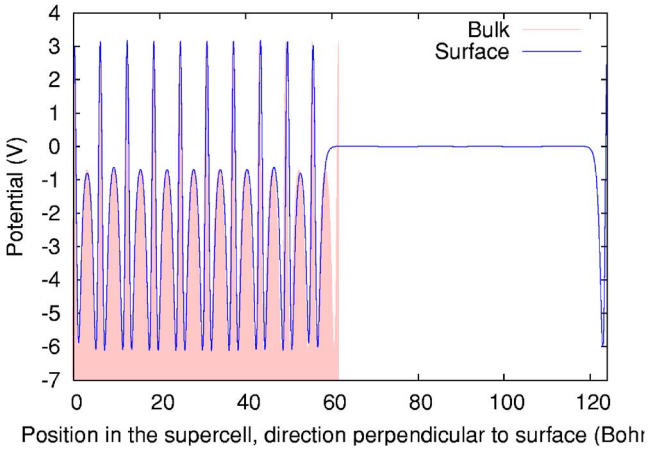

FIG. 4. (Color online) Electric potential averaged over the *x*-*y* plane as a function of the *z* position, for bulk (shaded region) and for the (110) surface (solid line).

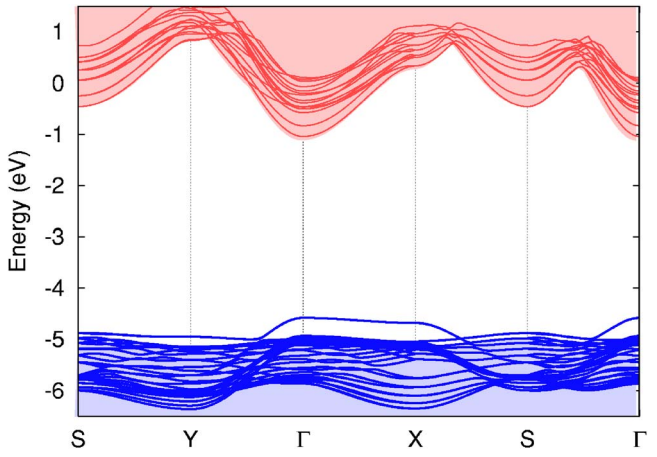

FIG. 5. (Color online) (110) surface band structure having the bulk band structure in the filled shadow.

Fig. 1. Again, the band gap is underestimated, so a shift to higher energies should be applied to the unoccupied states. Density of states were previously calculated by DiStefano[15] for the valence bands and by Satpathy *et al.*[16] The main feature when we compare our results with theirs is that the DOS of the valence bands in their case is split and so have three peaks, instead of the two we got. As was mentioned before, this is due to the use of relativistic approximations.

B. CsI surface

It is well known that polar surfaces are energetically unfavorable and even theoretically impossible because of divergent energy.[35] Nevertheless, these surfaces have been measured, and that is probably due to adatoms or surface defects that compensate the surface charge or to patchy areas of different charge on the surface. Also the divergence is surface energy is logarithmic in the crystal size, so small crystals may exist.[35] We simulated the (110) surface of CsI, which is nonpolar, and also the (100) surface, which is polar. To avoid the problem of an infinite surface charge in the polar surface, which in a supercell calculation leads to an electric field perpendicular to the surface, we built a surface with four unit cells, but alternatively terminating in a Cs and an I atom. This way we have charged planes, but in practice they form alternating dipoles and no net dipole perpendicular to the surface. It is not possible to build all possible types of (100)-oriented surfaces that lead to no net dipole, but this particular choice may give us an insight of what happens in general.

For the (110) surface, an orthorombic unit cell was used, consisting of a set of cells with four atoms each, built in such a way as to give the (110) orientation in the *z* direction. Then a column of such cells was built in the *z* direction. The number of cells was varied, and five such cells were found to be more than enough to guarantee that the central ones represent the bulk. **k**-point convergence was studied in this system, and a $8\times8\times1$ mesh was found sufficient to give converged total energies.

For the (100) surface four primitive unit cells in the *x*-*y* plane were used and sets of these four primitive unit cells

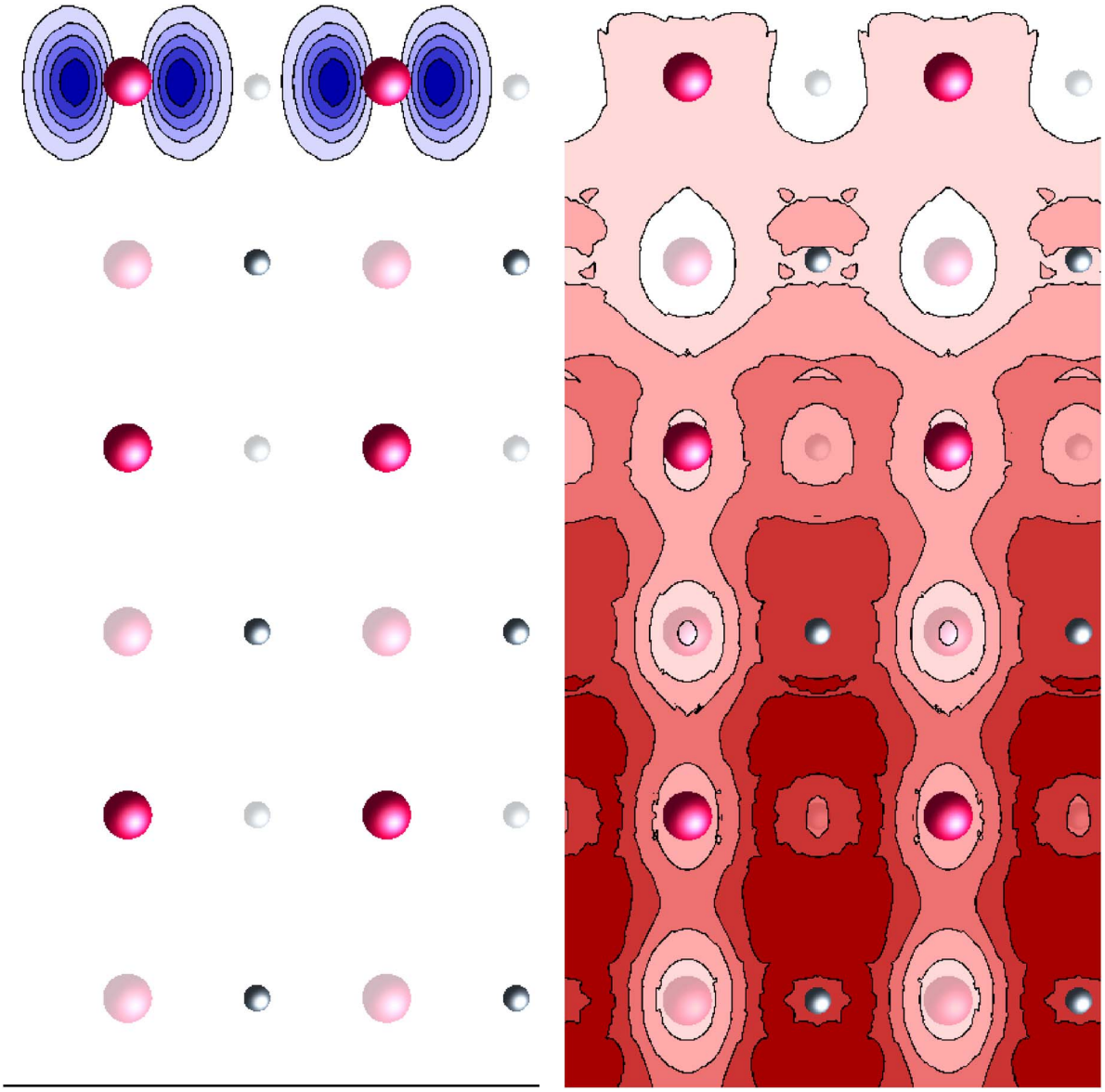

FIG. 6. (Color online) Modulus of the wave function at the Γ point for the surface sample: the left side shows the highest occupied level and the right side shows the lowest unoccupied level. The contour plot was taken on the plane halfway between the atoms shown at full and dim color. The small atoms are cesium while the large are iodine; dimmed atoms are behind the plane.

were added in the z direction, forming a column. Seven such sets were found to be more than enough to guarantee that the central ones represent the bulk. It can be seen that this way the surface is constructed with the outermost atoms being the cesium atoms in one of the two surfaces and the iodine atoms on the other surface. However, that would naturally create an electric field perpendicular to the surface and that surface is divergent in energy. Therefore we removed half of the Cs atoms from their surface and added them to the top of the I surface. This made two symmetry-equivalent surfaces that energetically do not diverge and so are possible. This will be referred to as the Cs surface. The alternative of removing I atoms from their surface and putting them on the top of the Cs surface was also done; this is the I surface.

The vacuum was obtained by increasing the supercell in the z direction to larger sizes than the volume with atoms. The x,y-plane-averaged electrostatic potential was calculated for both bulk and surface samples, and so the value of the flat potential in the vacuum was achieved. It allowed us to confirm that the volume of vacuum was enough to avoid interaction between atoms in different supercells. We found that a volume of vacuum of the same size as the five cells of atoms is more than good enough for the (110) surface (see Fig. 4), while seven were required for the (100) surface.

The atoms in the surface calculation were allowed to relax via a conjugate-gradient scheme until the energy change between subsequent iterations of structural optimization became less than 10^{-5} Ha.

In ionic solids like CsI, the electrostatic pair potentials dominate. This will lead to no direct mechanism to alter the two-dimensional symmetry of the surface, and so only movement of the atoms in the direction perpendicular to the sur-

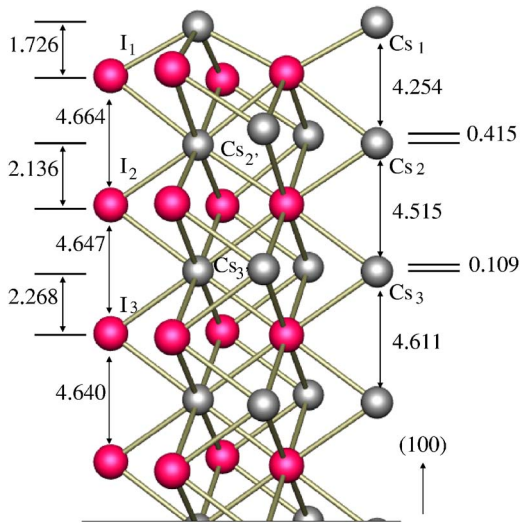

FIG. 7. (Color online) Diagram representing the relative displacements of the atoms of the Cs-terminated (100) surface after relaxation. There is a perspective effect to help the visualization, which distorts the image a bit.

face is expected.[36] This was observed in our simulations.

1. (110) surface

All the atoms of the sample with a surface were allowed to relax. Figure 2 shows the relative positions of the relaxed atoms, while Table III shows the distance the atoms on the sample deviated from their original positions. Relaxation happens as expected, with the topmost cesium ion receding into the bulk and the iodine ion moving towards the vacuum. This contradicts the results obtained by Butman *et al.*,[37] which suggest that the surface charge should be positive. Butman *et al.* do not know the orientation of their sample, but we suppose that the surface they were measuring was the (110) since it is the plane of easy cleavage.

Nevertheless, the relaxation is not large. Jockisch *et al.*[7] calculated the relaxation of the (110) CsI surface using a shell model and obtained a relaxation of the order of 1% for the outer layer. Jockisch *et al.* present a table with the positions of the core and the shell of the relaxed surface, and their results for the core are shown in Table III, together with our results. The direction of displacement of the cesium atoms is the same, although quantitatively the results are different. On the other hand, the direction of displacement of the iodine atoms is not always the same in both calculations. For most of the atoms, our calculations show a larger displacement. But both calculations predict the same direction of displacement of the atoms of the outer layer.

TABLE IV. Distances (Å) from the bulk equilibrium positions; a positive number means moving away from the surface towards the vacuum. The atom labels refer to the ones shown in Fig. 7.

Atom	Distance (Å)
Cs 1	−0.52
I 1	−0.05
Cs 2	−0.14
Cs 2′	0.23
I 2	−0.02
Cs 3	−0.02
Cs 3′	0.04
I 3	0.01

This relaxation affects the charge distribution near the surface. We calculated the Mulliken charge in each atom, and the result was used to determine the charge of each atom, which is shown in Fig. 3. The first three layers are clearly affected on their charges. The second-layer iodine atom accumulates negative charge at the expense of the first-layer iodine atom, but also of cesium atoms in the same layer. We observed that the surface not only produces localized states in the surface, but also in the layer just below the surface.

Figure 4 shows the electric potential averaged over the *x*-*y* plane as a function of the *z* position, for both bulk and the surface supercells. This graph allows us to conclude that the number of atoms in the *z* direction is sufficient to adequately describe both the bulk (central atoms) and the surface. Also, we can determine the vacuum level. The horizontal line on the right of the graph for the surface supercell also shows that the vacuum is adequately described and that no interaction between two adjacent slabs occurs. This graph was used in order to align the bands for Fig. 5. Only very little misalignment of the two graphs is observed near the surface, as would be expected by the small relaxation of this system.

Figure 5 shows the (110) surface band structure compared with the bulk (in the background). It can be seen that the surface creates a band in the band gap, with the electrons localized around the surface iodine atoms in *p*-type wave functions, centered on the iodine atoms (see also Fig. 6). The band gap is reduced to 92.7% of its value in the bulk due to this new band, even though the lowest unoccupied band recedes a bit towards higher energy.

Figure 6 shows the modulus of the wave function at the Γ point in a plane centered between the Cs and I atoms and

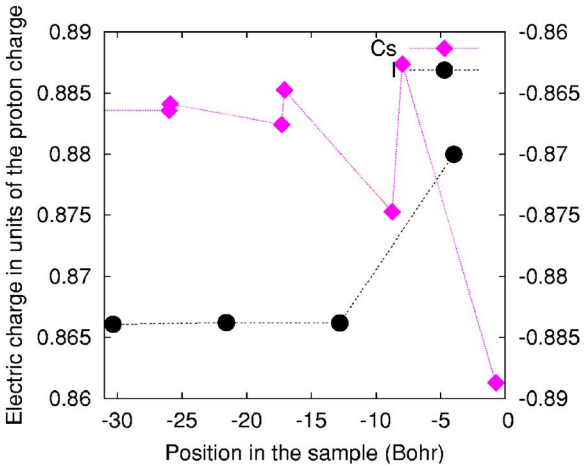

FIG. 8. (Color online) Charge state of Cs and I atoms, as a function of position in the material, as obtained from the Mulliken charge. The surface is at 0. The scale for iodine atoms is on the right and that for cesium atoms is on the left. The small atoms are cesium and the large ones iodine.

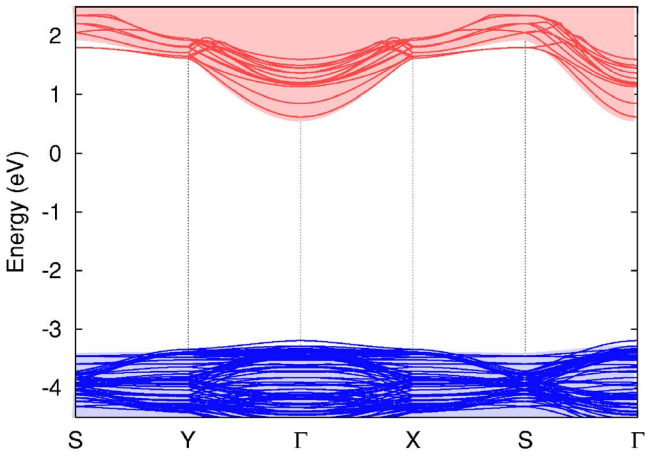

FIG. 9. (Color online) Surface band structure, with the bulk band structure as the filled region.

perpendicular to the surface. The left side of Fig. 6 shows the highest occupied level. It can be seen that it is localized on the surface, which confirms that the new band that appears in the band structure of Fig. 5 is indeed a surface state. We observed that all the occupied bands have their wave functions very localized near the cesium or iodine atoms, with the top ten localized near iodine atoms and of *p* type, which agrees with the nonconducting nature of CsI and the flatness of the occupied bands (Fig. 1). The highest occupied wave function at the Γ point is *p* type and points parallel to the surface in the (001) direction. On the other hand, the right side of Fig. 6 shows the lowest unoccupied state for the surface sample. It can be seen that it is highly delocalized and in the bulk of the sample. Again, this agrees with what is observed in the band structure.

2. (100) surface

Two types of (100) surfaces were studied: one with cesium-atom termination and another with iodine-atom termination. Figure 7 shows a diagram representing the relative relaxations of the atoms in the cesium-terminated (100) surface. The relaxation is very big, with atoms moving as much as half an Å, in the case of the outermost cesium atoms (see Table IV). Another interesting feature is the splitting of the second layer of cesium atoms into two layers, one with the atoms just below the surface cesium atoms and another with the other cesium atoms that do not have a surface cesium atom above. By contrast, the iodine atoms remain in the same plane.

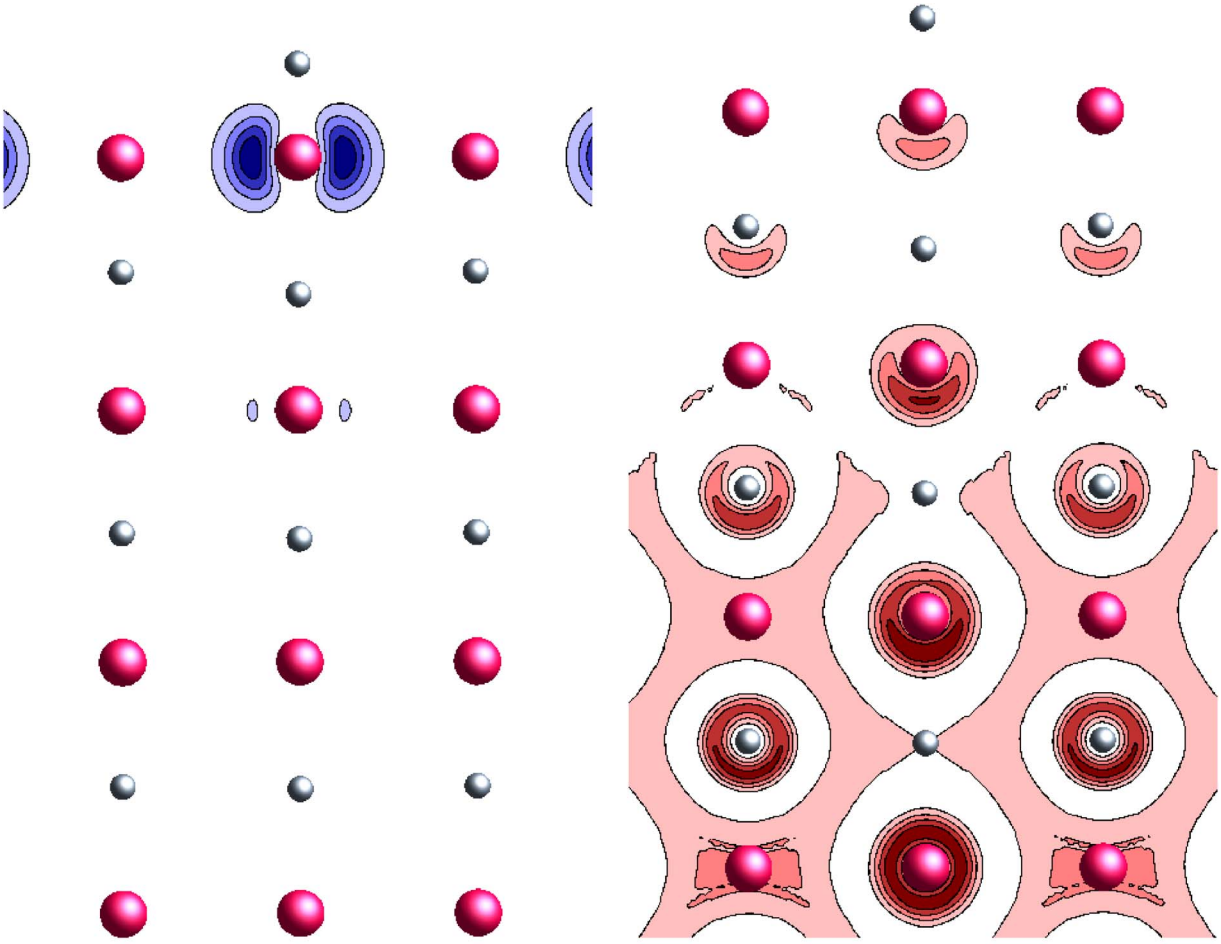

FIG. 10. (Color online) Modulus of the wave function at the Γ point for the surface sample: the left side shows the highest occupied level and the right side shows the lowest unoccupied level. The surface plot was taken at the surface near the Cs atom.

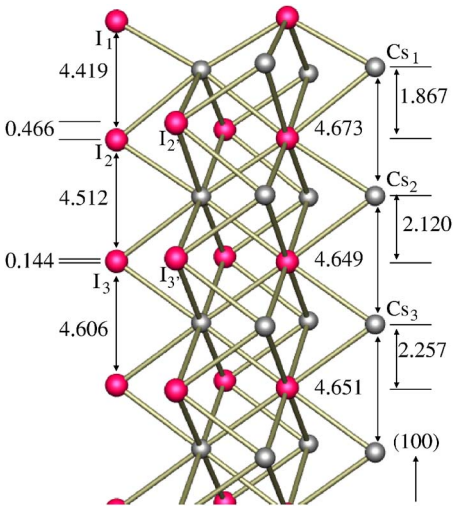

FIG. 11. (Color online) Diagram representing the relative motions of the atoms of the I-terminated (100) surface after relaxation. The most relevant atoms are marked. There is a perspective effect to help the visualization that distorts the image a bit.

The Mulliken charge was determined, and so the charge state of the atoms was obtained and is shown in Fig. 8. Since the iodine atoms remained in the same plane and actually with the same charge, there are only four points for iodine seen in the graph, while seven cesium points are shown. Besides, the iodine atoms all have about the same charge except for the ones nearest to the surface, while the cesium charge varies a lot, even for atoms in approximately the same plane parallel to the surface. The cesium atom on the surface in fact is less positive than the others, due to depletion of negative charge in the nearby iodine atom. In practice, this means that the surface cesium atom tends to be more electrically neutral than the cesium atoms in the bulk.

The electric potential averaged over the *x*-*y* plane as a function of the *z* position, for both bulk and the supercell, with a Cs surface was also calculated for this sample. This calculation showed that in this case the surface dramatically alters the potential—namely, by contracting the sample. For this reason, we had to use a larger sample in order to ensure that the number of atoms in the *z* direction is sufficient to adequately describe both the bulk (central atoms) and the surface. The vacuum level can also be determined using this calculation and was used in order to align the bands for Fig. 9.

TABLE V. Distances from the bulk equilibrium positions; a positive direction means moving away from the surface towards the vacuum. The atom labels refer to the ones shown in Fig. 11.

Atom	Distance (Å)
I 1	−0.39
Cs 1	0.07
I 2	−0.15
I 2′	0.27
Cs 2	0.03
I 3	−0.03
I 3′	0.07
Cs 3	0.02

The band structure of the (100) cesium surface is shown in Fig. 9. It is similar to the one obtained for the (110) surface in that a filled band appears in the gap near the highest occupied bulk band, although in this case it is much closer, so close that due to the increase in energy of the lowest unoccupied band, the band gap of this surface is actually slightly larger than the band gap of the bulk by 0.1%. The surface state band is of *p* type, pointing parallel to the surface and centered on the iodine atom, with alternating directions (110) and $(1\bar{1}0)$.

The modulus of the wave function for the Cs (100) surface is shown in Fig. 10. It is a cutaway view in the plane perpendicular to the surface that passes through a Cs surface atom. The highest occupied state is shown on the left; its *p*-type character can be seen in this picture. Its high localization on the near surface iodine atom is clear, in contrast with

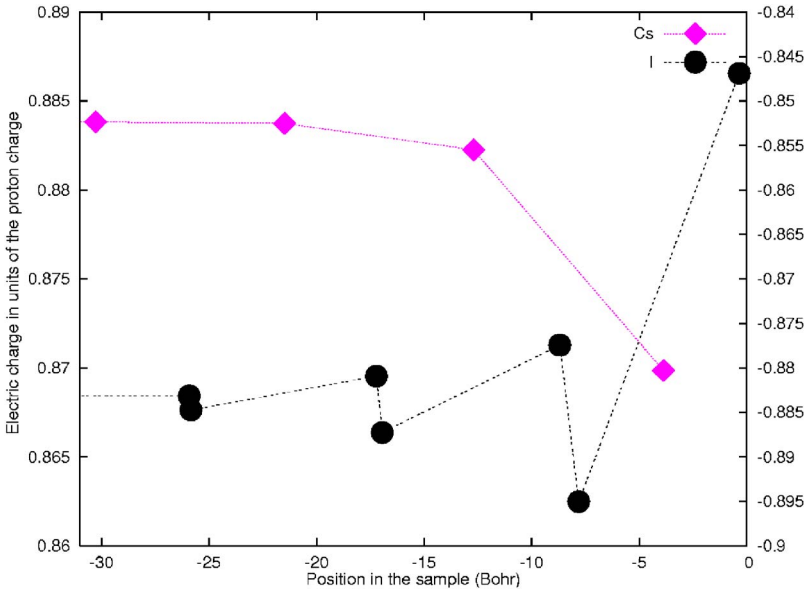

FIG. 12. (Color online) Charge of Cs and I atoms, as a function of position in the material, as obtained from the Mulliken charge. The surface is at 0. The scale for iodine atoms is on the right and for cesium atoms is on the left.

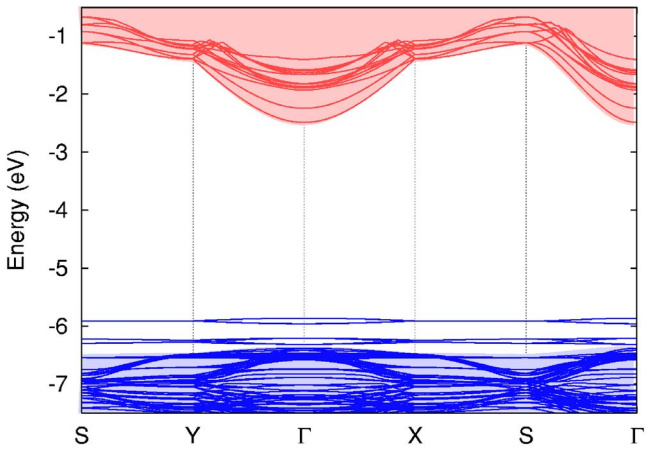

FIG. 13. (Color online) Surface band structure, with the bulk band structure as the filled region.

the delocalization of the lowest unoccupied state shown on the right, which is in the bulk of the material.

Figure 11 shows the iodine-terminated (100) surface. As with the Cs-terminated (100) surface, it is strongly compressed, although not as much. The movement of the atoms relative to their original positions is shown in Table V. Again, a distinction has to be made for the iodine atoms of the second plane, since the plane splits into two, with the atoms below the surface iodine atoms moving towards the bulk while the others (like I $2'$) move towards the vacuum. The distance between the cesium atoms does not change very much, and they remain in the same plane, as the iodine atoms did in the cesium-terminated (100) surface.

The ionic charge of the atoms near the iodine-terminated surface is shown in Fig. 12. The cesium charge is not constant, unlike the iodine on the cesium-terminated surface, and the variation in charge of the iodine ions is much larger in this case. The iodine atoms on the surface are more depleted of charge, and there is an alternating variation as we move towards the bulk.

The electric potential averaged over the *x*-*y* plane was again calculated, and the agreement between the curves in the center of the slab guarantees that we have a proper bulk region. The potential inside the sample is clearly lower for this iodine-terminated surface than in the other cases, relative to the vacuum level.

The most interesting result of the iodine-terminated (100) surface is the band structure, shown in Fig. 13. It can be seen that there are several bands created by the surface well inside the band gap. This reduces the band gap by 0.435 eV, a much larger difference than with the other types of surfaces.

Another interesting feature is shown in Fig. 14, where the modulus of the lowest unoccupied and highest occupied wave functions at the Γ point are shown. As expected, the highest occupied state is localized on the surface and is a

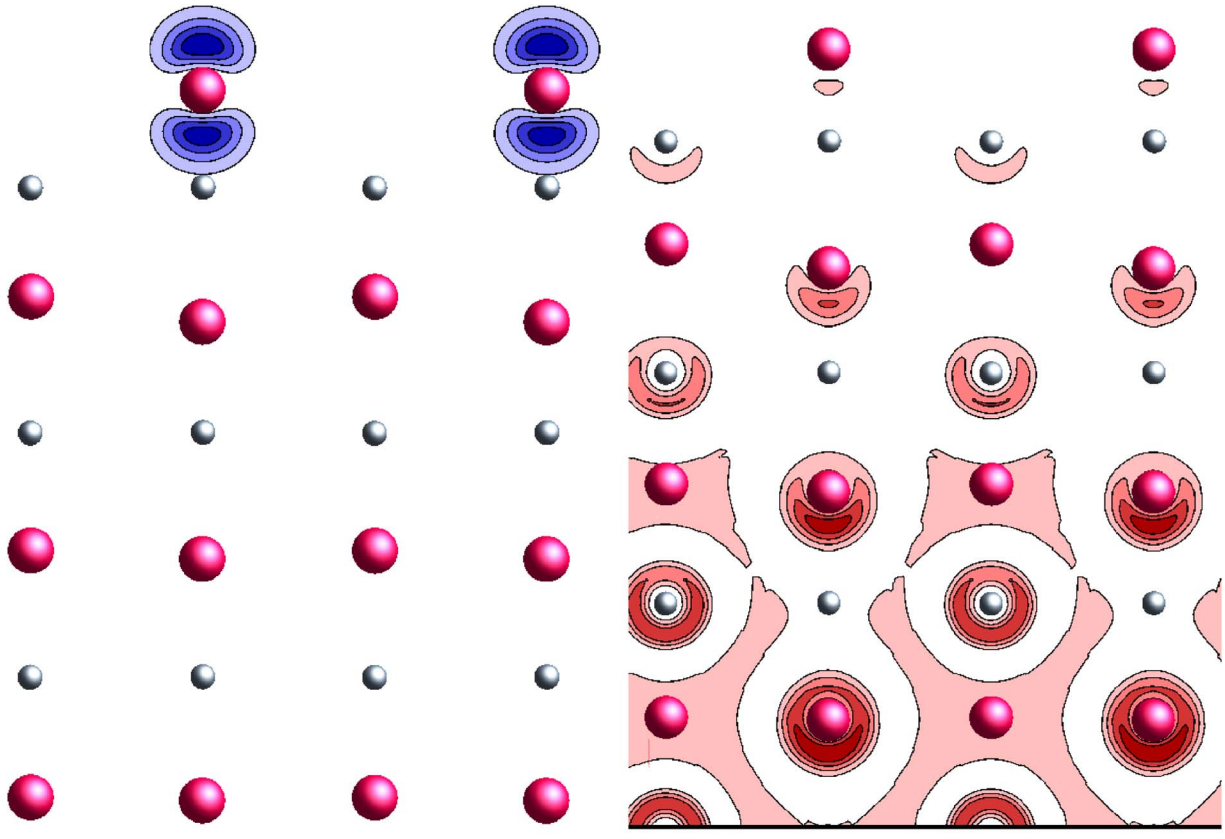

FIG. 14. (Color online) Modulus of the wave function at the Γ point for the surface sample: the left side shows the highest occupied level and the right side shows the lowest unoccupied level. The surface plot was taken at the surface near the I atom. The small atoms are cesium and the large ones iodine.

p-type wave function, but this time it points towards the vacuum, and therefore it is nondegenerate, as it is pointing along the symmetry axis. This will probably affect the reactivity of this surface. The levels below this one are also *p* type, degenerate, and pointing in the (100) and (010) directions.

IV. CONCLUSIONS

Bulk cesium iodine was studied using density functional theory. It was possible to have good agreement with experimental values for the lattice parameter, the bulk modulus, and the elastic constants, lending credibility to the technique for further studies. Three types of surface were studied, and relaxation parameters were calculated, as well as surface electronic states and charge. The results show little relaxation for the (110) surface, while for the cesium-terminated and iodine-terminated (100) surfaces, it is large. The creation of a surface generates states in the band gap, very close to the highest occupied band in the case of the cesium-terminated (100) surface and not so close for the iodine-terminated (100) surface. In this latter case, the *p*-type wave functions that appear on the surface point perpendicular to the surface, while in the case of the former they point parallel to the surface. This leads to the prediction of a much higher reactivity for the iodine-terminated surface. Calculations on the interaction of water with these surfaces are being performed which may give us a good idea of some degradation mechanisms of the CsI surface, important for radiation detectors.

ACKNOWLEDGMENTS

We wish to acknowledge the support of the Fundação para a Ciência e a Tecnologia (FCT) under Project No. POCI/FP/63442/2005, through POCI 2010, and FEDER. R.M.R. also wishes to acknowledge the FCT (ref. BSAB/466/2004) and the Fundação Calouste Gulbenkian for a grant to produce this work.

*Electronic address: ricardo@fisica.uminho.pt

[1] A. D. Mauro, Nucl. Instrum. Methods Phys. Res. A **525**, 173 (2004).
[2] C. Lu and K. T. McDonald, Nucl. Instrum. Methods Phys. Res. A **343**, 135 (1994).
[3] A. Breskin, Nucl. Instrum. Methods Phys. Res. A **371**, 116 (1996).
[4] A. Braem, M. Davenport, A. D. Mauro, P. Martinengo, E. Nappi, F. Piuz, and E. Schyns, Nucl. Instrum. Methods Phys. Res. A **515**, 307 (2003).
[5] H. Hoedlmoser *et al.*, Nucl. Instrum. Methods Phys. Res. A **553**, 140 (2005).
[6] A. Braem *et al.*, Nucl. Instrum. Methods Phys. Res. A **553**, 187 (2005).
[7] A. Jockisch, U. Schröder, F. W. de Wette, and W. Kress, Surf. Sci. **297**, 245 (1993).
[8] B. Winkler and V. Milman, J. Phys.: Condens. Matter **9**, 9811 (1997).
[9] P. Cortona, Phys. Rev. B **46**, 2008 (1992).
[10] S. Baroni and P. Giannozzi, Phys. Rev. B **35**, 765 (1987).
[11] S. Satpathy, Phys. Rev. B **33**, 8706 (1986).
[12] J. Aidun, M. S. T. Bukowinski, and M. Ross, Phys. Rev. B **29**, 2611 (1984).
[13] A. Ghosh and A. N. Basu, J. Phys. C **9**, 4365 (1976).
[14] Y. Onodera, J. Phys. Soc. Jpn. **25**, 469 (1968).
[15] T. H. DiStefano, Phys. Rev. B **7**, 1564 (1973).
[16] S. Satpathy, N. E. Christensen, and O. Jepsen, Phys. Rev. B **32**, 6793 (1985).
[17] K. Reinitz, Phys. Rev. **123**, 1615 (1961).
[18] D. I. Bolef and M. Menes, J. Appl. Phys. **31**, 1010 (1960).
[19] J. Vallin, O. Beckman, and K. Salama, J. Appl. Phys. **35**, 1222 (1964).
[20] Z. P. Chang, G. R. Barsch, and D. L. Miller, Phys. Status Solidi **23**, 577 (1967).
[21] G. Simmons and H. Wang, *Single Crystal Elastic Constant and Calculated Aggregate Properties* (MIT Press, Cambridge, MA, 1972).
[22] T. H. DiStefano and W. E. Spicer, Phys. Rev. B **7**, 1554 (1973).
[23] R. Jones and P. R. Briddon, *Semiconductors and Semimetals* (Academic Press, San Diego, 1998), Vol. 51A, Chap. 6, pp. 287–349, identification of defects in semiconductors.
[24] P. R. Briddon and R. Jones, Phys. Status Solidi B **217**, 131 (2000).
[25] J. P. Perdew, K. Burke, and M. Ernzerhof, Phys. Rev. Lett. **77**, 3865 (1996).
[26] C. Hartwigsen, S. Goedecker, and J. Hutter, Phys. Rev. B **58**, 3641 (1998).
[27] H. J. Monkhorst and J. D. Pack, Phys. Rev. B **13**, 5188 (1976).
[28] F. D. Murnaghan, Proc. Natl. Acad. Sci. U.S.A. **30**, 244 (1944).
[29] W. N. Mei, L. L. Boyer, M. J. Mehl, M. M. Ossowski, and H. T. Stokes, Phys. Rev. B **61**, 11425 (2000).
[30] G. R. Barsch and Z. P. Chang, *Accurate Characterization of the High Pressure Environment*, Natl. Bur. Stand. (U.S.) Spec. Pub. No. 326 (U.S. GPO, Washington D.C., 1971).
[31] M. Ross and A. K. McMahan, *Physics of Solids under High Pressure* (North-Holland, Amsterdam, 1981), p. 161.
[32] M. Ross, J. Chem. Phys. **56**, 4561 (1972).
[33] K. Asaumi, Phys. Rev. B **29**, 1118 (1984).
[34] U. Rössler, Phys. Status Solidi **34**, 207 (1969).
[35] A. M. Stoneham, in *Basic Science and Nuclear Divisions Fall Meeting* (The American Ceramic Society, New Orleans, 1979), pp. 54–64.
[36] F. W. deWette, W. Kress, and U. Schröder, Phys. Rev. B **32**, 4143 (1985).
[37] M. F. Butman, A. A. Smirnov, L. S. Kudin, and Z. A. Munir, Surf. Sci. **458**, 106 (2000).